Preprints.org

Article

Not peer-reviewed version

System Design and Launch of Hybrid Rocket with a Star-Fractal Swirl Fuel Grain Toward an Altitude of 15 km

Atsushi Takano *, Keita Yoshino, Yuki Fukushima, Ryuta Kitamura, Yuki Funami, Kenichi Takahashi, Akiyo Takahashi, Yoshihiko Kunihiro, Makoto Miyake, Takuma Masai, Shizuo Uemura

Posted Date: 30 May 2024

doi: 10.20944/preprints202405.2012.v1

Keywords: hybrid rocket; system design; star fractal swirl fuel grain; ballistic launch experiment; separation nut; telemetry; data logger

Preprints.org is a free multidiscipline platform providing preprint service that is dedicated to making early versions of research outputs permanently available and citable. Preprints posted at Preprints.org appear in Web of Science, Crossref, Google Scholar, Scilit, Europe PMC.

Copyright: This is an open access article distributed under the Creative Commons Attribution License which permits unrestricted use, distribution, and reproduction in any medium, provided the original work is properly cited.

Preprints.org (www.preprints.org) | NOT PEER-REVIEWED | Posted: 30 May 2024 doi:10.20944/preprints202405.2012.v1

Disclaimer/Publisher's Note: The statements, opinions, and data contained in all publications are solely those of the individual author(s) and contributor(s) and not of MDPI and/or the editor(s). MDPI and/or the editor(s) disclaim responsibility for any injury to people or property resulting from any ideas, methods, instructions, or products referred to in the content.

Article

System Design and Launch of Hybrid Rocket with a Star-Fractal Swirl Fuel Grain Toward an Altitude of 15 km

Atsushi Takano [1,*], Keita Yoshino [1], Yuki Fukushima [1], Ryuta Kitamura [1], Yuki Funami [2], Kenichi Takahashi [3], Akiyo Takahashi [3], Yoshihiko Kunihiro [4], Makoto Miyake [4], Takuma Masai [5] and Shizuo Uemura [5]

[1] Department of Mechanical Engineering, Kanagawa University, 3-27-1, Rokkakubashi, Kanagawa-ku, Yokohama, 221-8686, Japan; r202270180hc@jindai.jp (K.Y.); r202270160vl@jindai.jp (Y.F.); ft102093gj@kanagawa-u.ac.jp (R.K.)
[2] Department of Mechanical Engineering, National Defense Academy, 1-10-20, Hashirimizu, Yokosuka, Kanagawa, Japan; funami@nda.ac.jp
[3] Department of Aerospace Engineering, Nihon University, 7-24-1, Narashinodai, Funabashi, Chiba, Japan; takahashi.kennichi@nihon-u.ac.jp (K.T.); takahashi.akiyo@nihon-u.ac.jp(A.T.)
[4] Fullheart Japan Corporation, 3-20-8, Chuou, Ota-ku, Tokyo, Japan; y-kunihiro@fullheart.co.jp (Y.K.); m-miyake@fullheart.co.jp (M.M.)
[5] Research Institute for Engineering, Kanagawa University, Japan; zvu07747@nifty.com (T.M.); shiztomo@ybb.ne.jp (S.U.)
* Correspondence: atakano@kanagawa-u.ac.jp; Tel.: +81-45-481-5661 (ext. 3728)

Featured Application: Authors are encouraged to provide a concise description of the specific application or a potential application of the work. This section is not mandatory.

Abstract: To achieve low-cost and on-demand launches of micro satellites, the authors have been researching and developing a micro hybrid rocket since 2014. In 2018, a ballistic launch experiment was performed using the developed hybrid rocket, where it reached an altitude of about 6.2 km. The rocket engine had a 3D-printed solid fuel grain made of acrylonitrile butadiene styrene (ABS) resin in combination with a nitrous-oxide oxidizer. The fuel grain port had a star-fractal swirl geometry in order to increase the surface area of the port, to promote the laminar-turbulent transition by increasing the friction resistance, and to give a swirling velocity component to the oxidizer flow. This overcame the hybrid rocket's drawback of low fuel regression rate; i.e., it achieved a higher fuel-gas generation rate compared with a classical port geometry. In 2021, the hybrid rocket engine was scaled up and its total impulse was increased to over 50 kNs for reaching an altitude of 15 km. In addition to the engine, other components were also improved, such as through incorporation of lightweight structures, low-shock separation devices, a high-reliability telemetry device and data logger, while keeping costs low. The rocket was launched and reached an altitude of about 10.1 km, which broke the previous Japanese altitude record of 8.3 km for hybrid rockets. The presentation will report on the developed components from the viewpoint of system design and the results of the ballistic launch experiments.

Keywords: hybrid rocket; system design; star fractal swirl fuel grain; ballistic launch experiment; separation nut; telemetry; data logger

1. Introduction

Microsatellites have been actively developed [1,2]. However, except in the case that a large number of microsatellites are launched into the same orbit for constellation flight, these satellites are launched piggyback riding along with large satellites or released from the International Space Station;

© 2024 by the author(s). Distributed under a Creative Commons CC BY license.

Preprints.org (www.preprints.org) | NOT PEER-REVIEWED | Posted: 30 May 2024 doi:10.20944/preprints202405.2012.v1

thus, they have no choice of schedule or orbit. To launch these microsatellites quickly and at low cost, the authors have been developing of a micro hybrid rocket since 2014 and have conducted launch experiments every year until 2018. Hybrid rocket is consisted by liquid or gaseous oxidizer and a solid fuel like plastics or paraffins. Because the physical partition of fuel and oxidizer, hybrid rockets have high resistance to explosion hazards and can achieve safer and more reliable space transport systems compared to conventional liquid and solid rockets. Moreover, the safer character can realize low costs on ground manipulation on fuels and rockets, such as storage, production, transportation. Thus, many studies on hybrid rocket were conducted.

Because of a plastic grain like Acrylonitrile-Butadiene-Styrene (ABS) can be used for the fuel of hybrid rocket, many studies for 3-D Printed plastic grain. Lyne et al. developed powder fuel contained 3-D printed fuels to improve regression rate of the grain [30]. McFarland and Antunes conducted static combustion test 3D-printed grain made from ABS, acrylonitrile styrene acrylate, polylactic acid (PLA), polypropylene, polyethylene terephthalate glycol, Nylon, and PLA with aluminum particles to investigate the regression rate of the grain [31]. Wang et al. investigated combustion performance of fuels comprised a paraffin-based fuel embedded on a 3-D printed nested helical ABS grain [32].

Paraffins can also be used for the grain. Nakagawa et al. investigate a regression rate of five-type cylindrical port paraffin fuels with oxidizer swirl flow and concluded that the regression rate can be increased with oxidizer swirl flow [33]. Tang et al. investigated mechanical modified paraffin-based grain on combustion test to obtain an excellent paraffin-based grain with both good mechanical properties and combustion performance [34]. In 2017, the authors developed the 3D-printed solid fuel grain with a star-fractal port to improve the regression rate and used in the launch experiment. In 2018, the authors added swirl shape to a star-fractal port. The vehicle used star-fractal swirl port hybrid rocket engine launched in that year reached an altitude of 6.2 km [8]. In 2019, a 50 kNs-class hybrid rocket engine was developed with the goal of reaching a maximum altitude of 15 km; however, an engine rupture [9] occurred in combustion test hence the launch was abandoned. In 2020, COVID-19 prevented sufficient experiments from being conducted to determine the cause of the rupture failure, and the launch was abandoned again. In March 2021, the cause of the rupture was identified. An engine equipped with countermeasures successfully completed five combustion tests from May to July 2021, and a rocket named “Amanuma Maru” was launched at 6:00 am on September 19, 2021 from Noshiro City, Akita Prefecture. Atmospheric pressure telemetry data indicated that it reached a maximum altitude of 10.1 km. This paper reports a summary of its development and launch test.

2. Outline of the Rocket and the Launcher

Figure 1 is an overview of the rocket. Hybrid rocket propulsion has the propellant in different phase, i.e., liquid oxidizer and solid fuel, and has an essentially non-explosive nature due to its boundary layer combustion mechanism [10]. The reason for employing a hybrid rocket propulsion as our rocket engine is its high safety. The rocket was designed and developed in 2019 [11] and the launch was scheduled for 2019. However, several ruptures of the engine prevented the launch.

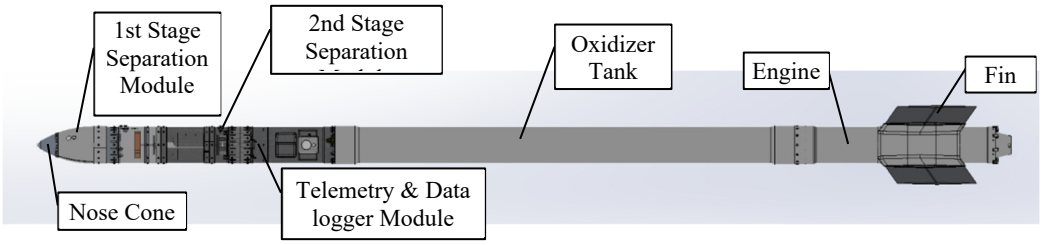

Figure 1. Overview.

An improved engine was subsequently developed and fitted. Table 1 shows its mass properties in comparison with those of CAMUI-500P [12], which held the altitude record for hybrid rockets in Japan, and our FY2018 model, “Fukushima-Maru”. The object of the development was to launch

Preprints.org (www.preprints.org) | NOT PEER-REVIEWED | Posted: 30 May 2024 doi:10.20944/preprints202405.2012.v1

microsatellites quickly and at low cost; thus, the method of manufacture used typical processing methods such as lathe processing and the vehicle was designed to be lightweight.

Table 1. Mass Properties.

Item	Unit	CAMUI-500P	FY2018 model, "Fukushima-Maru"[2]	FY2021 model, "Amanuma-Maru"
Gross liftoff mass, m_0	kg	68	37.3	57.1
Mass of the fuel before combustion, m_{f0}	kg	7.04[12]	3.60	7.84
Mass of the fuel after combustion, m_{ff}	kg	1.64[12]	0.97	1.73
Mass of the oxidizer, m_{ox}	kg	13.2[12]	13.0	24.0
Mass of the propellant, $m_p=(m_{f0}-m_{ff})+m_{ox}$	kg	18.6[12]	15.6	30.1
Propellant mass fraction $\zeta=m_p/m_0$	%	27.4	41.8	52.7

2.1. Engine

There is a technical issue in hybrid rocket propulsion – low fuel regression rate. This can cause low levels of thrust. To overcome this issue, many research and developments were conducted. For example, Fuller et al. developed and studied a grain with a star swirl port [13,14]. Whitmore et al. developed and studied a grain with a circular helical port [15,16]. Yuasa et al. studied the improvement of the regression rate of hybrid rockets by a swirling oxidizer flow [17,18]. The authors also developed a 3D-printed solid fuel grain with a grain with a star-fractal [19], cherry-blossom-fractal [19] and a star-fractal swirl port was developed [20]. Figure 2 shows the cross-section of the port has star-fractal geometry, and it is swept while rotating axially. The purposes of the star-fractal swirl port are to have a large surface area and to generate a swirling oxidizer flow. The effectiveness of this port was demonstrated in ground combustion experiments [21], the improvement of the regression-rate of the fuel was evaluated [22], and hence this port was adopted for the launch experiment.

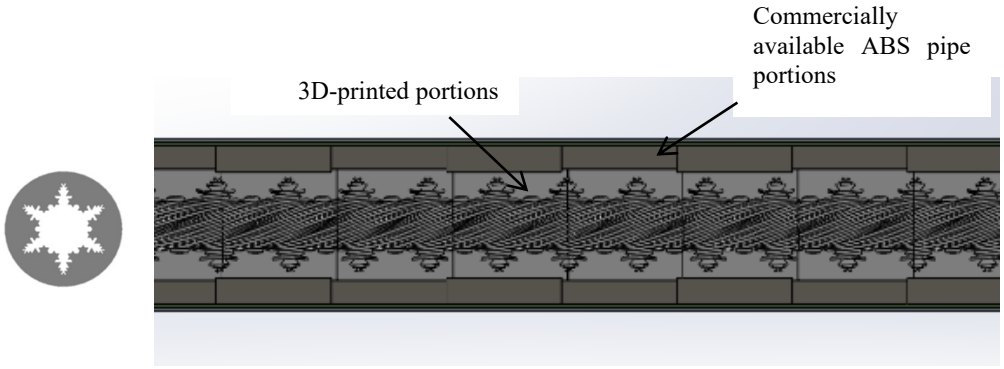

Figure 2. Star Fractal Swirl Shaped Port.

The fuel grain was made by a fused-deposition-modeling-type, commercial-grade 3D printer. The filament material of the 3D printer was an acrylonitrile butadiene styrene (ABS) resin. Because 3D printing was a time-consuming process, only portions near the port were 3D-printed. Commercially available ABS pipes were used as other portions of the fuel grain. This also led to cost reductions.

Preprints.org (www.preprints.org) | NOT PEER-REVIEWED | Posted: 30 May 2024 doi:10.20944/preprints202405.2012.v1

The fuel grain was covered by a glass-fiber-reinforced-plastics (GFRP) ablator and inserted into a motor case. There were two types of motor cases, such as the external thread type and the welded flange type. These motor cases were different only for the fastening method between the motor case and the injector, and between the motor case and the nozzle housing. For these motor case, however, their function as a combustion chamber was the same by design. The oxidizer, nitrous oxide (N_2O), was injected into the combustion chamber through the injector. The bell nozzle was made by graphite and had a 31 mm throat.

The development of the engine was started in 2019. The preliminary model was designed, developed, and tested. However, several ruptures occurred in the combustion test. Their cause was determined to be self-decomposition of the oxidizer, nitrous oxide [23] and insufficient strength of the resin housing of the nozzle. Improvements made to both the oxidizer and housing prevented the rupture. Figure 3 shows combustion test facility, which was also improved to have enough strength to prevent failure on engine rapture. Figure 4 shows the thrust and time curve of the five successful combustion tests, and Table 2 confirms the reproducibility of the total impulse (integration of thrust and time curve), which was within -5.0% to +5.1% of the average.

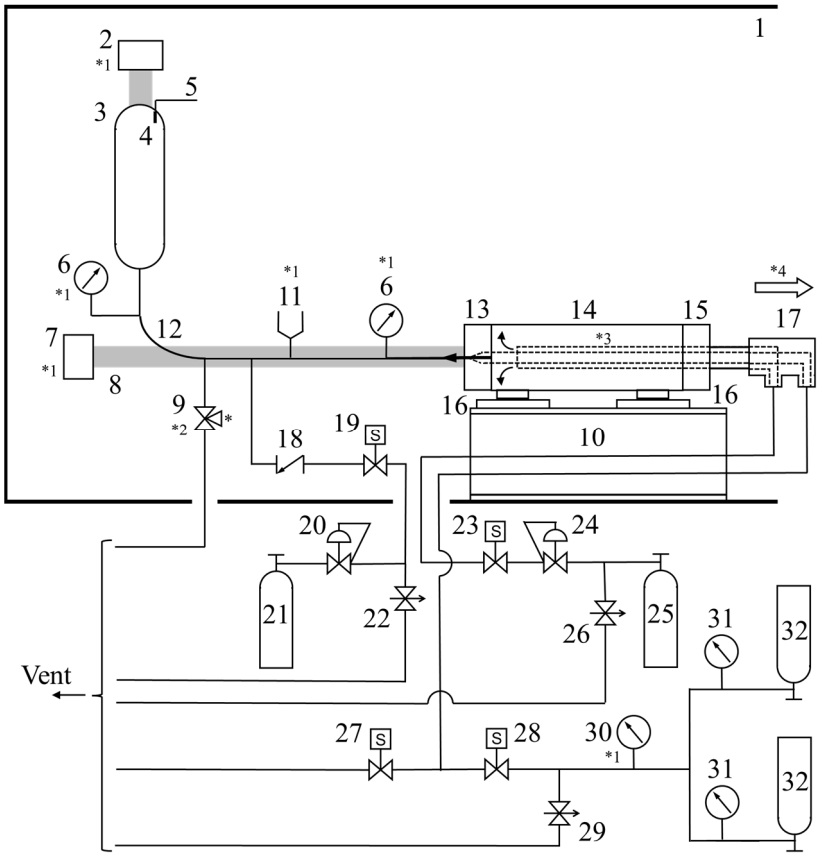

Note:
*1 The measured data were recorded using a LR8400, whose sampling period was 10 ms, made by Hioki E. E. Corporation.
*2 The exit * of the three-way valve (9) was not used.
*3 Two nichrome wires were attached to the stem (17).
*4 After ignition, the stem (17) was ejected.

1	Freight container
2	Load cell for measuring tank weight (9E01-L3-50K, NEC San-ei Instruments, Ltd.)
3	Oxidizer tank
4	Brass pipe for controlling amount of oxidizer in tank
5	Vent port
6	Pressure transducer (SSV-010MP-02, Sayama Corporation)
7	Load cells for measuring thrust (TCLA-20kNB, Tokyo Measuring Instruments Laboratory Co., Ltd. and 9E01-L3-5T, NEC San-ei Instruments, Ltd.)
8	Thrust transmitting column
9	Three-way valve for discharging oxidizer in the tank

Preprints.org (www.preprints.org) | NOT PEER-REVIEWED | Posted: 30 May 2024 doi:10.20944/preprints202405.2012.v1

10	Engine stand (H-section steel)
11	Sheathed type K thermocouple (HTK0222, Hakko Electric Co. Ltd.)
12	Flexible hose
13	Injector bell
14	Motor case
15	Nozzle housing and graphite nozzle
16	Linear motion guide
17	Launch stem
18	Clack valve of N_2 Line
19	Solenoid valve of N_2 Line
20	N_2 regulator
21	N_2 cylinder
22	Needle valve for manual depressurization of N_2 line
23	Solenoid valve of O_2 Line
24	O_2 regulator
25	O_2 cylinder
26	Needle valve for manual depressurization of O_2 line
27	Solenoid valve for N_2O dumping
28	Solenoid valve for N_2O filling
29	Needle valve for manual depressurization of N_2O line
30	Pressure gauge (GC-31-174, Nagano Keiki Co. Ltd.)
31	Pressure gauge (PGI-63-MG10-LAQX, Swagelok Co.)
32	N_2O cylinder

Figure 3. Combustion test facility.

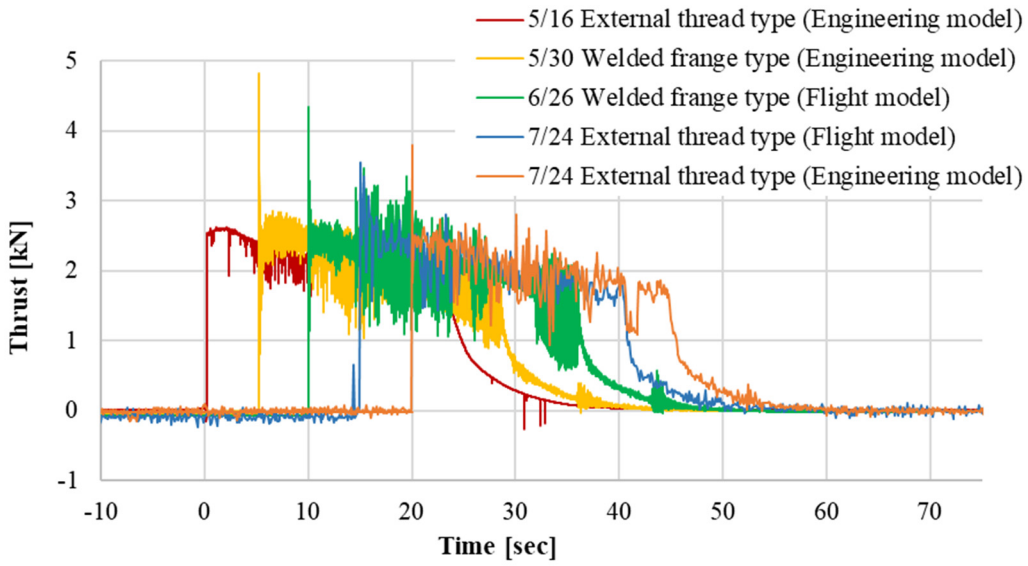

Figure 4. Comparison of Thrusts.

Table 2. Comparison of Total Impulse, I_t.

Motorcase type	External thread (S/N01)	Welded frange (S/N01)	Welded frange (S/N03)	External thread (S/N02)	External thread (S/N01)	Average
Test date	May 16	May 30	Jun 26	Sep 24	Sep 24	
Total impulse [kNs]	56.6	51.2	55.2	53.1	56.0	53.9
Difference from average [%]	5.1	-5.0	2.5	-1.4	3.9	-
Thrust measuring method	Estimated from combustion pressure	Measured by load cell	Measured by load cell	Measured by load cell	Measured by load cell	-

Preprints.org (www.preprints.org) | NOT PEER-REVIEWED | Posted: 30 May 2024 doi:10.20944/preprints202405.2012.v1

2.2. Oxdizer Tank

The oxidizer tank is based on the one developed in 2018 [24]. The total length was extended to 2 m to increase the carrying capacity. Due to extended length and the difference in the coefficient of thermal expansion between the aluminum alloy body and the carbon fiber reinforced plastic (CFRP) that reinforces it, the CFRP reinforcement part cracked as a result of the temperature drop during the filling of the tank with the oxidizer. The part was subsequently improved by changing the lamination sequence. As a result, the weight index $pV/(mg)$ (maximum internal pressure × volume / tank weight) was improved 1.7 times, i.e., from 1.4 to 2.4.

2.3. Separation Mechanism

As shown in Figure 1, the rocket had separation mechanisms on the first and second stages. The purpose the separation mechanism of the first stage is to release a streamer to slightly decelerate the rocket at the top of its flight, while that of the second stage is to release the parachute and deployable floats to further decelerate the rocket and land on the sea. The first-stage separation mechanism used a Nichrome wire to cut Reny (high performance polyamide based on mainly polyamide MXD6) bolts, which is a type of polyamide resin. This mechanism had been used in launches in 2016, 2017, and 2018. The second-stage separation mechanism used a non-explosive low-shock separation mechanism [25] with a separation nut.

2.4. Telemetory & Datalogger

Telemetry measured air pressure and GPS position coordinates during flight, and it downlinked to the ground by using LoRa (Long Range) communication protocol, a type of LPWA (Low Power Wide Area) using 920 MHz-band. The data logger recorded information, such as acceleration, geomagnetism, and gyro, and was picked up when the rocket was recovered. Both units were mounted on the measurement module shown in Figure 1. Because the altitude of the rocket can be estimated from the air pressure during flight, it can be measured in real time from the downlink signal. The GPS signal was used to identify the position of the rocket when it landed on sea. The telemetry and data logger had initially been developed at Kanagawa University and flew in 2017 [26] and 2018 [27]; they were made more compact, lightweight and reliable by Fullheart Japan Company [28].

2.5. Body

The strength design was taken into account for a compression load by thrust load of rocket engine, bending load by wind gust, and shock load by parachute opening. To achieve ultra-lightweight, the body was constructed by thin-walled, composite material cylinders. The critical failure load of the thin-walled cylinders is buckling due to compression load. It is well-known that the experiment buckling load has large scatter and is smaller than the theoretical buckling load. The ratio, the experimental buckling load divide by the theoretical buckling load, is called "Knockdown factor". Many efforts to find the cause of the difference between the experimental buckling load and the theoretical buckling load have been conducted. The cause, however, is not revealed. One of the authors, Takano, derived the theoretical buckling load with less approximation for composite cylinder [29,30] and, obtained the statistical knockdown factor with confidence bound [31]. The method by the theoretical buckling load with the statistical knockdown factor was applied for the design of the body hence it achieved ultra-light weight body. Divergence (static divergence due to aeroelasticity) of the fuselage was also taken into consideration in the design of the bending stiffness fuselage and the joints (couplers) between the stages. CFRP was used for the body material that achieves high-bending stiffness, and glass fiber reinforced plastic (GFRP) was used for the body of the equipment that generated radio waves, such as the measurement module. The coupler was fixed to the fuselage with shear bolts. However, because it is difficult to predict the rigidity reduction of the joint, the bending stiffness of the fuselage was measured to determine the stiffness reduction of

Preprints.org (www.preprints.org) | NOT PEER-REVIEWED | Posted: 30 May 2024 doi:10.20944/preprints202405.2012.v1

the joint and it was used to evaluate the divergence. An internal resonance phenomenon, which was studied by Wang and Chan [32], was not considered. Thus, the consideration is the future work.

2.6. Fin & Finstay

Flutter, which is an aeroelastic phenomenon, was also considered in the design of the fins and fin stays (L-clip that fixes the fins to the body). The fins had a diamond airfoil cross section and an aluminum honeycomb sandwich panel with a CFRP skin to improve stiffness. To avoid a decrease in stiffness in the fin stay, which is the joint between the fin and the body, an L-clip made of CFRP was used and both adhesion and peeling bolt joints were used.

2.7. Launcher [33]

The launcher had a glide length of 12 m with elevation angle from 60° to 86° and was designed for the maximum rocket weight of 100 kg and rocket length of 5 m. The maximum elevation angle error due to elastic deformation by the 150kg weight of rocket was designed less than 0.55°. It was designed to be divided into pieces of 3.6 m or less in length to enable it to be moved to the launch site, with most parts being 20 kg or less in weight; thus it could be assembled without the need for heavy machinery. Design load for the launcher was not only the rocket weight but also wind loads. Design load by wind for a crane design standard [34] was applied. For the operational state, which was elevation angle with 80° and set the rocket, 16m/s was applied and the minimum margin of safety (MS) was 5.5. For non-operational state, which was elevation angle 0° and without the rocket, 56m/s was applied and the minimum MS was 0.45.

3. Launch Test and Results

A launch test was conducted at 6:00 am on September 19, 2021 at the former Ochiaihama in Noshiro City, Akita Prefecture, for the purpose of a flight demonstration and attempting to break the Japanese altitude record for hybrid rockets. Figure 5 shows the state of launch.

Figure 5. Moment of Launch.

The oxidizer filled by GSE (Ground Support Equipment) shown in Figure 3. without freight container, engine stand and linear motion guide.

From the visual observation by telescope camera and the altitude data described later, it was judged that the combustion of the engine was normally complete. Altitude data from the atmospheric pressure telemetry was also successfully received. The launch was planned to be carried out on any day with good weather from September 18th to 20th, 2021, including the backup date. However, due

Preprints.org (www.preprints.org) | NOT PEER-REVIEWED | Posted: 30 May 2024 doi:10.20944/preprints202405.2012.v1

to the effects of Typhoon No. 14, which took a peculiar course of going from western Japan to eastern Japan after staying in the East China Sea, the launch was postponed on the 18th as it was judged that the sea swells were high and the navigation and recovery work of the recovery ship would be difficult. On the 19th, it was forecast that swells would remain on the sea the day before, but there was a risk that the launch on the 20th would fail due to problems with the rocket and GSE. Therefore, a final decision was made based on the weather at 4:00 AM on the 19th. Although the land was covered with fog, the surface of the sea could be seen from the vicinity of the launch point, and so it was decided to proceed with the launch. After inserting the rocket into the launcher, it became possible to turn on the power of the on-board camera; however, there was a problem that recording could not be started with the remote control.

Condensation on the day of the flight was severe and the video cameras on the ground also had condensation inside the camera lens. Thus, the condensation was judged to be the cause of the problem. If the recording of the camera mounted on the rocket could not start, it would not be possible to shoot videos during flight. However, it was judged that the purpose of the experiment could be achieved even if the camera recording was not possible, so it was decided to launch the rocket. As shown in Table 3, just before launch, one of the two atmospheric pressure telemetry units and one GPS telemetry unit were out of communication. However, previous experience had indicated that the position of the antenna and the position of the receiving station could be improved depending on the attitude of the rocket, so the launch proceeded. An investigation after the flight indicated a possible cause was that the GPS and atmospheric pressure telemetry had been unable to be received before the launch because of the carrier sense function, which stops radio waves when radio waves are emitted in the same frequency band near the transmitter to avoid interference.

Table 3. Telemetry condition of the launch test.

Time	GPS		Atmospheric pressure		Forced separation	
	24ch	31ch	38ch	45ch	52ch	59ch
5:40	○	×	×	○	○	○
6:00 (before launch)	○	×	×	○	○	○
6:00 (on launch)	×	×	×	○	×	×

GPS reception became impossible after the launch, but this seems to be due to restricted GPS reception for high-speed moving objects. However, there was also a problem that communication with the forced separation circuit became impossible, and it was not possible to confirm the voltage supply signal to the Nichrome wire for separation or receive the separation signal.

Investigations conducted after flight determined the cause to be forced separation circuit failure due to condensation or low temperatures under 0 ℃ at high altitude.

However, only atmospheric pressure telemetry was received. Figure 6 shows the result of estimating the altitude from the atmospheric pressure data.

Preprints.org (www.preprints.org) | NOT PEER-REVIEWED | Posted: 30 May 2024 doi:10.20944/preprints202405.2012.v1

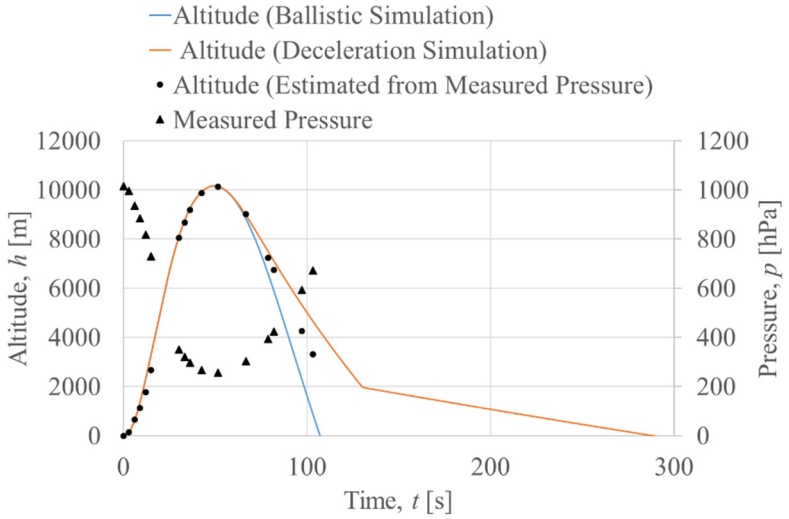

Figure 6. Pressure and Altitude.

Altitude was estimated using the height measurement formula (Equation (1)) derived from the ICAO (International Civil Aviation Organization) standard atmosphere. Note that the subscript 0 means the ground value. As a result of calculation using the pre-launch pressure p_0 =1014.42 hPa, temperature T_0 =13 ℃, and the minimum measured atmospheric pressure p_0 =256.85 hPa, the maximum attainable altitude was calculated to be 10124 m. This means the flight broke the previous altitude record of 8.3 km (estimated value) held by CAMUI-500P.

$$H = \frac{\left\{1-\left(\frac{p}{p_0}\right)^{\frac{1}{5.2561}}\right\}(T_0+273.15)}{0.0065} \tag{1}$$

Figure 5 also shows the altitude simulation results. The data after the apex show ballistic fall (fall without streamer and parachute deployed) and deceleration fall (fall with streamer and parachute deployed). Considering this result and the fact that the separation signal could not be received, it is thought that the first stage did not separate normally and fell, landing on the water before the second stage separation. As a result of subsequent investigations, the cause was determined that a forced separation circuit failure had occurred due to dew condensation and a drop in temperature at high altitudes.

Velocities also evaluated by the altitude simulation results and numerical differentiation of measured height. The numerical differentiation is second-ordered, using three measured point shown in Equation (2).

$$y_1'(2) = \frac{1}{1+n}\left\{\frac{y_3-y_2}{x_3-x_2}+n\frac{y_2-y_1}{x_2-x_1}\right\} \quad ; \quad n=\frac{x_3-x_2}{x_2-x_1} \tag{2}$$

Figure 7 shows the measured and simulated velocity. The maximum velocities of height direction are 309 m/s (measured) and 290 m/s (simulated). The possibility cause of the difference is prediction accuracy of drag coefficient (C_d) of the rocket. C_d was predicted by the following step. Calculating C_d on the subsonic (Mach=0.8) and then predicting C_d change by Mach number (Mach-C_d) was using data of similar rocket. Thus, the C_d around Mach=1 has less accuracy. Improvement of the Mach-C_d is the future work.

Preprints.org (www.preprints.org) | NOT PEER-REVIEWED | Posted: 30 May 2024 doi:10.20944/preprints202405.2012.v1

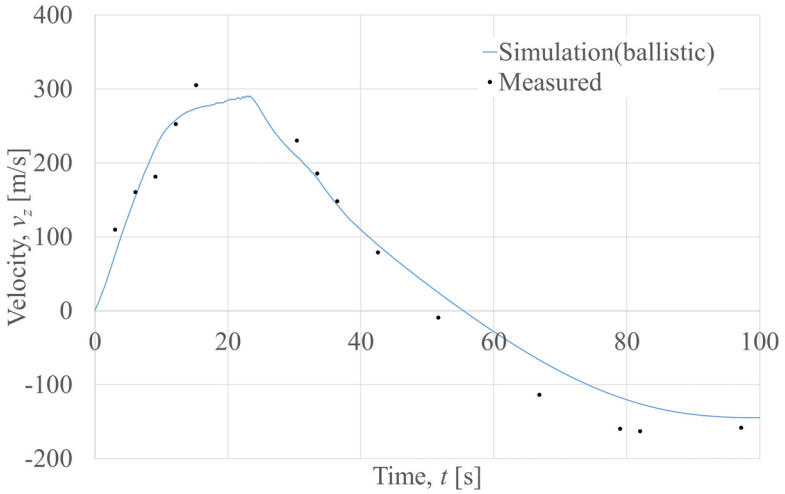

Figure 7. Comparison of velocity.

4. Conclusion

A hybrid rocket was launched and achieved an altitude of 10.1 km, setting a new domestic altitude record for hybrid rockets. However, the confirmation of the separation signal, the reception of the GPS signal, and the recovery of the rocket failed, and the data of the on-board data logger could not be recovered. Furthermore, it is presumed that the first stage did not separate normally either. Although the domestic altitude record for hybrid rockets was broken, many problems remained. An investigation conducted after flight revealed the cause of the failure of the telemetry and forced separation circuits. In the future, we would like to take countermeasures against these problems and improve the attainable altitude.

Author Contributions: Conceptualization, At.T.; methodology, At.T. and F.Y.; software, R.K., Y.K. and M.M.; investigation, At.T., K.Y. Y.F. and R.K.; data curation, X.X.; writing—original draft preparation, At.T.; writing—review and editing, At.T., K.T., Ak.T., T.M. and S.U.; project administration, At.T. All authors have read and agreed to the published version of the manuscript.

Funding: Not applicable.

Institutional Review Board Statement: Not applicable.

Informed Consent Statement: Not applicable.

Data Availability Statement: The data presented in this study are available on request from the corresponding author. The data are not publicly available due to the fact they are not open data.

Conflicts of Interest: Author Yoshihiko Kunihiro and Makoto Miyake were employed by the company Fullheart Japan Corporation. The remaining authors declare that the research was conducted in the absence of any commercial or financial relationships that could be construed as a potential conflict of interest.

References

1. Microsatellites from UNISEC, UNISEC homepage, http://unisec.jp/unisec/satellites, (accessed Feb. 13th, 2024).
2. Shou, H.N. Micro-Satellite Configuration of Discoid and Asymmetrical, Gyroless with Thrusters Three-Axis Robust Control and Stability Analysis, *International Journal of Engineering and Technology Innovation*, **2014**, 1, 1-17.
3. Lyne, J. E.; Brigham, A.; Savery, R.; Karcher, K.; Pyron, J.; Adams, L.; Reagan, G.; Furches, H.; Sola, D.; Melendez, L.; Keck, C.; The Use of a 3-D Printed, Polymer Matrix Containing Pulverized Fuel in a Hybrid Rocket, AIAA Propulsion and Energy Forum, 2018, DOI: 10.2514/6.2018-4597.
4. McFarland, M.; Antunes, E. Small-Scale Static Fire Tests of 3D Printing Hybrid Rocket Fuel Grains Produced from Different Materials, Aerospace, 2019, 6, 81.

Preprints.org (www.preprints.org) | NOT PEER-REVIEWED | Posted: 30 May 2024 doi:10.20944/preprints202405.2012.v1

5. Wang, Z.; Lin, X.; Li, F.; Yu, X. Combustion performance of a novel hybrid rocket fuel grain with a nested helical structure, Aerospace Science and Technology, 2020, 97, 105613.
6. Nakagawa, I.; Hikone, S.; Ishiguro, T.; Maruyama, S. A Study on Paraffin-based Fuel Hybrid Rockets, Trans. JSASS Aerospace Tech. Japan, 2012, 10, ists28, To_1_7-To_1_10.
7. Tang, Y.; Chen, S.; Zhang, W.; Shen, R.; DeLuca, L. T.; Ye, Y. Mechanical Modifications of Paraffin-based Fuels and the Effects on Combustion Performance. Propellants Explosives Pyrotechnics, 2017, 42, 1268-1277, DOI:10.1002/prep.201700136.
8. Takano, A.; Funami, Y.; Nishino, S. Conceptual design and launch of hybrid rocket with star fractal swirl fuel grain. *UNISEC Space Takumi Journal*, **2020**, 9, 1-16 (in Japanese).
9. Igarashi, H.; Takano, A.; Kitamura, R, Funami, Y. Burst case of hybrid rocket engine with nitrous oxide and countermeasures. 10th UNISEC Space Takumi Conference, **2020**, UNISEC 2020-004 (in Japanese).
10. Takahashi, A.; Shimada, T. Essentially non-explosive propulsion paving a way for fail-safe space transportation. *Transactions of the JSASS, Aerospace Technology Japan,* **2018**, 16, pp. 1-8.
11. Bao, J.; Kitamura, R.; Takano, A, Funami Y, "Conceptual design of a hybrid rocket toward an altitude of 15km. 2nd Hybrid Rocket Symposium, **2019**, HR-2019-006 (in Japanese).
12. Nagata, H.; Wakita M.; Totani T.; Uematsu T. Development and Flight Demonstration of 5kN Thrust Class CAMUI Type Hybrid Rocket. *Transactions of the JSASS, Aerospace Technology Japan,* **2014**, 12, Ta 1-Ta 4.
13. Fuller, J-K.; Ehrlich, D.A.; Lu, P. C**.,** Jansen, R. P**.,** Hoffman, J. D. Advantages of Rapid Prototyping for Hybrid Rocket Motor Fuel Grain Fabrication. *AIAA Paper* 2011-5821, **2011**.
14. Armold, D.; Boyer, J. E.; Kuo, K. K.; DeSain, J. D.; Curtiss, T. J.; Fuller, J. K. Test of Hybrid Rocket Fuel Grains with Swirl Patterns Fabricated Using Rapid Prototyping Technology. *AIAA Paper* 2013-4141, **2013**.
15. Whitmore, S.A.; Walker, S.D.; Merkley, D.P.; Sobbi, M. High Regression Rate Hybrid Rocket Fuel Grains with Helical Port Structures. *J. Propul. Power,* **2015**, 32, 1727–1738.
16. Whitmore, S.A.; Walker, S. D. Engineering Model for Hybrid Fuel Regression Rate Amplification Using Helical Ports. *J. Propul. Power,* **2017**, 33, 398–407.
17. Yuasa, S.; Shimada, O.; Imamura, T.; Tamura, T.; Yamamoto, K. A Technique for Improving the Performance of Hybrid Rocket Engines. *AIAA Paper* 1999-2322, **1999**.
18. Yuasa, S.; Shiraishi, N.; Hirata, K. Controlling Parameters for Fuel Regression Rate of Swirling-Oxidizer-Flow-Type Hybrid Rocket Engine. *AIAA Paper* 2012-4106, **2012**.
19. Tateyama, T.; Takano, A. Development of CFRP Reinforced Lightweight Hybrid Rocket Engine. *Aerospace Technology Japan,* **2018**, 17, 237–243 (in Japanese).
20. Shizume, M.; Takano, A.; Funami, Y.; Morohoshi, H.; Tahara, K.; Terada, T. Development of Hybrid Rocket Engine with Star Fractal Swirl Grain Made by 3D Printer. Space Transportation Symposium FY2017, Sagamihara, Japan, STPC-2017-012, **2018** (in Japanese).
21. Funami, Y.; Takano, A. Ground combustion experiments of hybrid rocket fuel grain with a star fractal swirl port. 63rd Space Sciences and Technology Conference, 2E07 (JSASS-2019-4316), **2019** (in Japanese).
22. Funami, Y.; Takano, A. Regression-Rate Evaluation of Hybrid-Rocket Fuel Grain with a Star-Fractal Swirl Port. *Trans. Japan Soc. Aero. Space Sci*. **2023**, 66, 61–69.
23. Hamazaki, A.; Kaneyori, H.; Masu, K.; Kumada, K.; Funami, Y.; Kitamura, R.; Takano, A. Investigation of decomposition on nitrous oxide for hybrid rocket engine. Proceedings of Space Transportation Symposium FY2020, STCP-2019-013, 2021 (in Japanese).
24. Tateyama, T.; Takano, A. Development of Low Cost / Light Weight Oxidizer Tank in Hybrid Rocket. *Aerospace Technology Japan,* **2020**, 19, 19-26 (in Japanese).
25. Takano, A.; Nishino, S. Development of Separation Mechanism Using Non-Explosive Separation Nuts. *Aerospace Technology Japan,* **2020**, 19 179-185 (in Japanese).
26. Shimazaki, T.; Takano, A. Development of Telemetry device and Launch result at Izu Oshima. 8th UNISEC Space Takumi Conference, UNISEC 2018-003, **2018**(in Japanese).
27. Yoshida, M.; Shimazaki, T.; Takano, A. Development and flight test result of telemeters for hybrid rocket. Space Transportation Symposium FY2018, STCP-2018-024, **2019** (in Japanese).
28. Hoshi, T.; Takano, A.; Miyake, M.; Kunihiro, Y. Development of independent mounting type Telemetry device for micro launch vehicle. 10th UNISEC Space Takumi Conference, UNISEC 2020-003, **2020** (in Japanese).
29. Takano, A. Improvement of Flügge's Equations for Buckling of Moderately Thick Anisotropic Cylindrical Shells, *AIAA Journal*, **2008,** 46, 903-911.
30. Takano, A. Simple Closed-Form Solution for the Buckling of Moderately Thick Anisotropic Cylinders, *Trans. JSASS, Aerospace Technology Japan*, **2012**, 10, 17-26.
31. Takano, A. Statistical Knockdown Factors of Buckling Anisotropic Cylinders under Axial Compression, *ASME Journal of Applied Mechanics*, **2012**, 79, 051004, doi: 10.1115/1.4006450.
32. Wang, Y.R.; Chang, Y.S. Study of Primary and Internal Resonance on 3D Free-Free Double-Section Beam. *Adv. technol. innov.*, **2020**, 5, 270–291.

Preprints.org (www.preprints.org) | NOT PEER-REVIEWED | Posted: 30 May 2024 doi:10.20944/preprints202405.2012.v1

33. Tachibana, Y.; Yamaguchi, Y.; Takano, A. Development of 12 m launcher for 5 m hybrid rocket launch. Proceedings of Space Transportation Symposium FY2018, TCP-2018-025, **2019** (in Japanese).
34. Japanese Industrial Standards Committee, Cranes-Wind load assessment, *JIS B 8830*, **2001**. +5

Disclaimer/Publisher's Note: The statements, opinions and data contained in all publications are solely those of the individual author(s) and contributor(s) and not of MDPI and/or the editor(s). MDPI and/or the editor(s) disclaim responsibility for any injury to people or property resulting from any ideas, methods, instructions or products referred to in the content.